LANGMUIR

pubs.acs.org/Langmuir Article

# Urea Glass Route as a Way to Optimize YAGG:$Ce^{3+}$,$Cr^{3+}$,$Pr^{3+}$ Nanocrystals for Persistent Luminescence Applications

Vitalii Boiko,* Maria Luisa Saladino,* Francesco Armetta, Federica Ursi, Marta Markowska, Karina Grzeszkiewicz, Cecilia Mortalò, Cristina Leonelli, and Dariusz Hreniak

Cite This: *Langmuir* 2022, 38, 11539−11549 Read Online

ACCESS | Metrics & More | Article Recommendations | Supporting Information

**ABSTRACT:** A new approach for the synthesis of $Y_3Al_2Ga_3O_{12}$ (YAGG) nanophosphors allowing the preparation of crystallites with sizes starting from 45 nm is presented. The controllability of the energy and trap density of the resulting material samples by annealing temperature was confirmed by thermoluminescence (TL) measurements. It has been shown that the annealing of samples at temperatures up to 1300 °C does not cause any substantial growth of crystallites, still remaining below 100 nm, but leads to changes in the activation energy of the persistent luminescence (PersL) process. On the other hand, annealing above 1400 °C results in grain growth on the submicron scale, which was confirmed by X-ray powder diffraction (XRPD) and electron transmission microscopy (TEM) measurements. In addition, with an increase in the molar ratio of urea to the total amount of metals used ($R$), qualitative changes are observed in the PersL process occurring from the excited states of $Cr^{3+}$ and $Pr^{3+}$ ions. This proves the influence of the synthesis process, in particular of the metal complexation at its initial stage, on the final structure ordering in the annealed materials. These observations are linked to previously reported defects in the YAGG structure, leading to PersL.

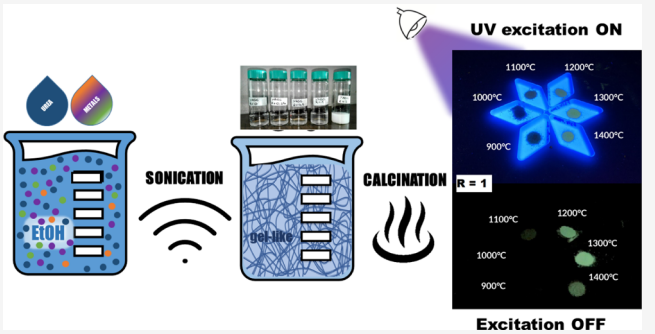


## INTRODUCTION

In recent years, great interest in nanomaterials has been observed due to their enormous potential in fundamental studies and the technological field. In this broad class of nanomaterials, an important role is played by luminescent nanoparticles and, in particular, by those activated by trivalent lanthanide ions, due to their promising applications in the fields of bioimaging, lighting, optical nanothermometry, and solar concentrators.[1−3]

Many research groups around the world are strongly motivated to develop not only new hosts for such phosphors but also new synthetic routes to obtain them in the well-defined nanomaterial form.[4−11] It is well known that the physical properties of crystalline materials are highly dependent on the host material, phase purity, grain size distribution, and crystalline homogeneity. Over the years, mixed oxide systems have been of particular interest due to their stability and design potential for a wide range of properties, such as energy gaps, mainly through ion replacement. In the next step, of course, it is necessary to provide specific properties and the final form of the material, respectively, by appropriate doping and selection and optimization of their synthesis method.[12−14]

One of the most promising materials intensively investigated in recent years in various research centers is yttrium aluminum gallium garnet (YAGG, $Y_3Al_2Ga_3O_{12}$), which exhibits specific luminescent properties after appropriate doping.[15,16] The crystal structure of YAGG is shown in Figure 1. The structure belongs to the space group $Ia\bar{3}d$. The general chemical formula of an oxide garnet is $X_3A_2B_3O_{12}$, where X refers to a dodecahedral site, A to an octahedral site, and B to a tetrahedral site. The garnet structure has many edges shared between adjacent polyhedra; each tetrahedron and octahedron share edges with two or six dodecahedra, while each dodecahedron divides edges with two tetrahedra, four octahedra, and four other dodecahedra; finally, tetrahedra and octahedra are connected to each other from all angles.[17] Gilleo and Geller reported that aluminum and gallium prefer tetrahedral sites,[17] but the reasons are different. Aluminum is located in a four-coordinate site due to the small radius, while the preference of gallium to the tetrahedral site is explained by the nature of $Ga^{3+}$ rather than by the effect of the radius. In fact, the ions with electronic configuration $d^{10}$ tend to settle according to $sp^3$ hybridization, preferring the tetrahedral site.[18]

Received: March 21, 2022
Revised: August 22, 2022
Published: September 13, 2022







https://doi.org/10.1021/acs.langmuir.2c00687
*Langmuir* 2022, 38, 11539−11549

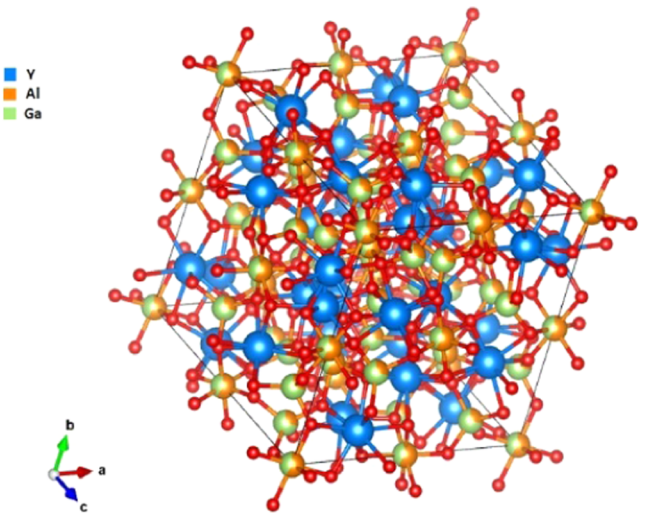


**Figure 1.** $Y_3Al_2Ga_3O_{12}$ structure.

YAGG doped singly or codoped with $Cr^{3+}$ is known as one of the new so-called persistent phosphors, which exhibit continuous luminescence for a long duration (minutes, hours, or days) after ceasing the excitation source.[19−22] Most recent studies are devoted to nanophosphors emitting in the red and near-infrared (NIR) regions.[23−25] Although YAGG with such properties could be obtained by its codoping with $Cr^{3+}$ and other trivalent ions, the intensity and duration of persistent luminescence (PersL) in the red region cannot compete with green and blue ones.[19] PersL in the red region can be used in biomarkers for in vivo imaging, temperature sensing, and security marks in bonds and banknotes.[9,26,27] Polycrystalline YAGG codoped with $Cr^{3+}$ and $Ce^{3+}$ (YAGG:$Ce^{3+}$,$Cr^{3+}$) has been intensively studied by the Tanabe group.[19,21,28] The introduction of $Cr^{3+}$ to YAGG:$Ce^{3+}$ was proposed for obtaining long PersL of $Ce^{3+}$ at room temperature. Furthermore, YAGG nanopowders can also be used as a starting material for the production of high-quality optical ceramics with PersL properties, which can be used, for example, in optical storage applications.[29]

The addition of a third dopant to this system allows obtaining new red and near-infrared phosphors, which are of current interest,[30−32] preferably broad bands excited by blue LEDs. Some doping ions such as $Nd^{3+}$, $Pr^{3+}$, and $Yb^{3+}$ have been successfully used to obtain emissions through efficient energy transfer (ET) from $Ce^{3+}$ and $Cr^{3+}$.[33,34] In previous works, optimal dopant ratios were already investigated for both spectral properties[35] and PersL effects.[36] Special attention has been given to the investigation of the mechanism involved in persistent luminescence,[37−39] which is correlated to the size and aggregation of particle or lattice defects. Recently, we reported particle size-related limitations of persistent phosphors based on the nanocrystalline YAGG obtained by the Pechini method[30] and coprecipitation method.[40] It was found that although at higher annealing temperatures, the properties of the resulting phosphors do not change significantly, the smaller crystallites obtained exhibit more surface defects that can lead to PersL quenching. Therefore, the goal of this study was to investigate the controllability of the energy and trap density of $Y_3Al_2Ga_3O_{12}$:$Ce^{3+}$,$Cr^{3+}$, $Pr^{3+}$ while better maintaining the nanometric size and uniform morphology of particles. To this aim, the urea glass route (UGR) method was chosen for their synthesis, followed by annealing at several temperatures in the range of 900−1400 °C. This one-pot, green, and time-saving synthetic method has already been developed for the preparation of nitride nanoparticles[41] and Ce:YAG nanopowders[42] and allows the preparation of materials with high control of powder purity, crystalline structure, and morphology. According to the UGR procedure, metallic salts are solubilized in ethanol, and after the addition of urea, they form a so-called gel-like phase. Urea in ethanol can form complexes with many metals, usually through the carbonyl group or, in the case of more soft metals, with the nitrogen of the amino group. The gel-like phase is the result of the ability of urea to form a polymeric-like organization, which is able to accommodate the nuclei that form during the subsequent heat treatment. Thanks to the formation of an intermediate "gel-/glass-like" material, the primary nanoparticles are stabilized during the heat treatment.

## EXPERIMENTAL PART

**Materials.** Urea (Acros Organics, 98%), ethanol (Aldrich, 99.98%), $Y(NO_3)_3{\cdot}6H_2O$ (Aldrich, 99.8%), $Al(NO_3)_3{\cdot}9H_2O$ (Aldrich, 98%), $Ga(NO_3)_3{\cdot}9H_2O$ (Aldrich, 99.9%), $Pr_6O_{11}$ (Sigma-Aldrich, 99.99%), $Ce(NO_3)_3{\cdot}6H_2O$ (Aldrich, 99.99%), $Cr(NO_3)_3{\cdot}9H_2O$ (Fluka 97%) were used in the paper.

**Preparation of Nanocrystals.** YAGG codoped with $Ce^{3+}$, $Cr^{3+}$, and $Pr^{3+}$ nanocrystals were synthesized following this procedure. A solution containing $Al(NO_3)_3{\cdot}9H_2O$, $Y(NO_3)_3{\cdot}6H_2O$, $Ga(NO_3)_3{\cdot}9H_2O$, $Pr_6O_{11}$, $Ce(NO_3)_3{\cdot}6H_2O$, and $Cr(NO_3)_3{\cdot}9H_2O$ salts in ethanol was prepared in a (Y + Ce + Pr)/(Al + Cr)/Ga molar ratio of 3:2:3 by setting the concentration of $Y(NO_3)_3$ as 0.12 mol $L^{-1}$ to obtain the following formula $Y_{2.9865}Ce_{0.006}Pr_{0.0075}Al_{1.9875}Cr_{0.0125}Ga_3O_{12}$. An appropriate amount of urea was added to the ethanolic solution with metals to obtain urea/

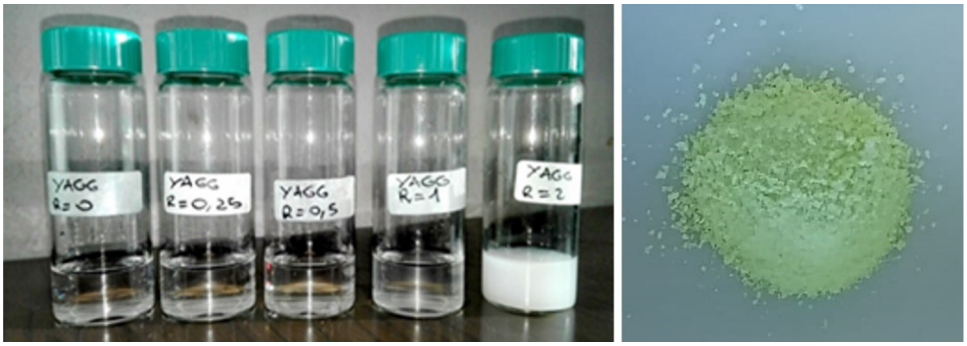


**Figure 2.** Systems obtained by the urea glass route with urea/metal molar ratios, *R*, of 0, 0.25, 0.5, 1, and 2 (left). Image of the $Ce^{3+}$-, $Cr^{3+}$-, $Pr^{3+}$-codoped powder (right).



https://doi.org/10.1021/acs.langmuir.2c00687
Langmuir 2022, 38, 11539−11549

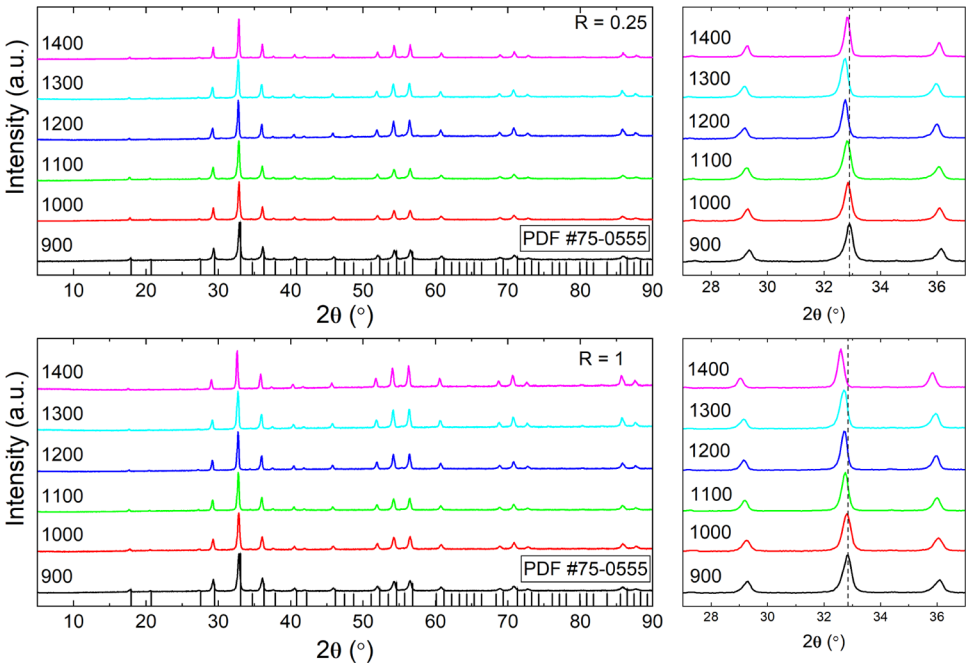


**Figure 3.** XRD patterns of the YAGG:$Ce^{3+}$,$Cr^{3+}$,$Pr^{3+}$ powder obtained with the UGR method with $R$ = 0.25 and 1 calcined in the range of 900−1400 °C. The reference pattern (PDF#75-0555) is reported at the bottom.

metal molar ratios, $R$, of 0, 0.25, 0.5, 1, and 2. The obtained systems were subjected to agitation in an ultrasonic bath for 20 min to obtain homogeneous and transparent dispersions identifiable with a gel-like system, as can be observed in Figure 2.

For $R$ > 1, the formation of a white dispersion was observed, which separates within a few hours. White dispersion may be associated with the decomposition of urea; for this reason, for the correct purposes of the present paper, only systems with $R$ < 1 are suitable. This study was thus performed by calcining only two systems at $R$ = 0.25 and 1 for 1 h at temperatures of 900, 1000, 1100, 1200, 1300, and 1400 °C. The system at $R$ = 0.5 was not treated and deeply studied because of a few differences in behavior observed between $R$ = 0.25 and 1 (see the Results and Discussion section). After the heat treatment, the powders appear green (Figure 2).

**Characterization Techniques.** *X-ray powder diffraction (XRPD).* XRPD patterns were acquired by a Philips PW 1050/39 diffractometer in the Bragg−Brentano geometry using Ni-filtered Cu K$\alpha$ radiation ($\lambda$ = 1.54056 Å) in the 2$\theta$ range of 5−90° with a step of 0.05° and a time for the step of 5 s. The X-ray generator worked at a power of 40 kV and 30 mA, and the resolution of the instrument (divergent and antiscatter slits of 0.5°) was determined using R-$SiO_2$ and R-$Al_2O_3$ standards free from the effect of reduced crystallite size and lattice defects. The phase identification has been performed using X′pert HighScore Software. To obtain information about phase composition, cell parameters, and the crystalline size of the phases, XRPD patterns were analyzed according to the Rietveld method using MAUD software.[43,44].

*Transmission Electron Microscopy (TEM).* TEM micrographs of YAGG:$Ce^{3+}$,$Cr^{3+}$,$Pr^{3+}$ nanophosphors annealed at 900, 1000, and 1100 °C were acquired using a JEM-2100 (JEOL, Japan) microscope operating at an accelerating voltage of 200 kV. Each powder was homogeneously dispersed in isopropanol by sonication for 2 min. A drop of the suspension was deposited on a lacey carbon grid of 300 mesh, and after complete solvent evaporation, the grid was introduced into the TEM chamber for analysis. TEM micrographs of YAGG:$Ce^{3+}$,$Cr^{3+}$,$Pr^{3+}$ nanophosphors annealed at 1200 and 1400 °C were acquired using a last-generation high-resolution scanning/transmission electron (S/TEM) microscope (Thermo Scientific Talos F200S) equipped with energy-dispersive X-ray spectroscopy (EDS) and operating at an accelerating voltage of 200 kV. Samples were homogeneously dispersed in bidistilled water (Millipore) by sonication for 10−15 min. A drop of each suspension was deposited on a copper grid of 200 mesh coated with a transparent polymer (Formvar/carbon) and then dried. Subsequently, specimens were carbonated (carbon coater: Balzers CED-010) for TEM investigations.

*Photoluminescence Emission (PL) and Excitation (PLE) Spectra.* Photoluminescence emission (PL) and excitation (PLE) spectra as well as photoluminescence lifetime (microsecond range) were measured using an FLS980 Fluorescence Spectrometer from Edinburgh Instruments. As an excitation source, a 450 W xenon lamp (for PL and PLE) and a 150 W xenon pulse lamp (for a lifetime) were used. An R928P side window photomultiplier tube from Hamamatsu was used as a detector. Both the excitation and emission 300 mm focal length monochromators were in the Czerny Turner configuration. The excitation arm was supplied with a holographic grating of 1800 lines $mm^{-1}$, blazed at 300 nm, while the emission arm was supplied with ruled grating, 1800 lines $mm^{-1}$ blazed at 500 nm. The scanning range was from 250 to 680 nm for PLE spectra and from 460 to 820 nm for PL spectra. For external quantum yield (QY) measurements, an integrating sphere (SM4 from Edinburg Instruments) with a diameter of 30 cm was additionally used. In this case, the signal intensity on the sample was about 60 mW.

The photoluminescence lifetime (nanosecond range) was carried out using a femtosecond laser setup composed of a Coherent Libra-S all-in-one ultrafast oscillator and a regenerative amplifier laser system, with a pulse duration of less than 100 fs at a 1 kHz repetition rate, a Coherent OPerA-Solo optical parametric amplifier, and a Hamamatsu C5677 streak camera with a time resolution of 14 ps.

*Thermoluminescence (TL).* Thermoluminescence (TL) curves were measured with a lexsygresearch TL/OSL reader (Freiberg Instruments GmbH, Freiberg, Germany). The signal was collected with an R13456 PMT (Hamamatsu Photonics) monitoring the global emission from the whole spectral response (from 185 to 980 nm) with an integration (channel) time of 0.1 s. A blue laser diode PL450B ($\lambda_{max}$ = 450 nm, FWHM = 2 nm, power 1 mW $cm^{-2}$) by Osram was used as an irradiation source. To learn more about the properties of the traps contributing to the main thermoluminescent peaks, the $T_{max}$−$T_{stop}$ (partial cleaning) experiment proposed by McKeever was performed.[45] The method involved the following procedure: the sample was irradiated at room temperature, partially heating the sample to temperature $T_{stop}$, cooling to room temperature, and


https://doi.org/10.1021/acs.langmuir.2c00687
Langmuir 2022, 38, 11539−11549

reheating to record (heating rate 0.5 °C $s^{-1}$) all of the remaining glow curves. Positions of the first maximum $T_{max}$ in the glow curve versus $T_{stop}$ were plotted in the $T_{stop}$ range between 30 and 150 °C with a step of 10 °C to cover completely the glow curve. These studies were complemented by an initial rise analysis.[46] All modules were controlled by LexStudio 2, and the obtained data were processed with Origin software.

## RESULTS AND DISCUSSION

**Structure and Morphology.** The structure of codoped YAGG samples was studied by XRPD. The XRPD patterns of the samples with $R$ = 0.25 and 1 treated at various temperatures are shown in Figure 3.

All XRPD patterns are constituted by a single garnet phase[47,48] and are in good agreement with that of YAGG. The transformation from amorphous to the stable phase garnet occurs completely with heat treatment at a relatively low temperature (900 °C). No additional diffraction peaks were observed, thus indicating the absence of any secondary phases. All diffraction peaks became narrower with increasing temperature, which indicates the higher crystallinity of the powder. This behavior could be attributed to the particle size increase or the strain effect, which could also contribute to the peak broadening of the XRPD patterns. The diffraction patterns were simulated by the Rietveld refinement analysis. For each sample, the agreement between the experiment and the model was evaluated by $R_b$ (4−6%) and the curve of residues. The cell parameter $a$ and the size of crystallites $D$ obtained for each sample are given in Figure 4.

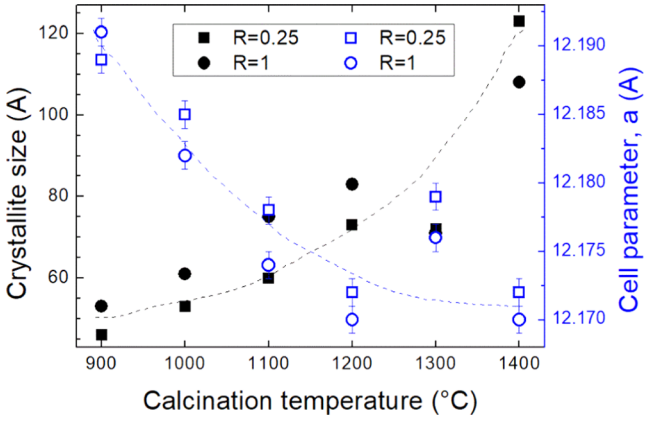


**Figure 4.** Cell parameter, $a$, and crystallite size, $D$, obtained for YAGG:$Ce^{3+}$,$Cr^{3+}$,$Pr^{3+}$ with $R$ = 0.25 and 1 and calcined for 1 h in a temperature range of 900−1400 °C. Dashed lines are a guide for eyes only.

The obtained values of the cell parameter $a$ are in agreement with the hypothesis of $Al^{3+}$ replacement with $Ga^{3+}$, in agreement with Vegard's law, and are due to the difference in ionic radii (Ga(III) = 0.76 Å and Al(III) = 0.53 Å).[48] The cell parameter of undoped YAG is 12.008 Å, while the ones of yttrium gallium garnet (YGG) when all aluminum ions are substituted with gallium is 12.270 Å.[44] $Ga^{3+}$ ionmainly occupies 24d lattice sites and $Al^{3+}$ occupies 16a lattice sites.[47,48] The ratio between the octahedral (16a) and tetrahedral (24d) is equal to 2:3. $Ce^{3+}$ and $Pr^{3+}$ ions partially substitute $Y^{3+}$ ions, while $Cr^{3+}$ ions replace aluminum ions in the octahedral position.[49]

As the analysis of the diffraction patterns of the two series showed no significant differences between the cell parameter, $a$, and the crystallite size, $D$, subsequent studies thus focused on the effect of temperature. During the heat treatment, urea has been decomposed releasing gaseous products that do not interfere with the formation of the garnet phase but result in possible defects or in formation of small particles. In both cases, $R$ = 0.25 and 1, the decrease in the cell parameter with increasing annealing temperature can depend on a homogeneous disorder introduced into the lattice during the amorphous to crystalline transformation and on an imperfect local stoichiometry, which causes an increase in the lattice parameter.

On the other hand, the treatment at a higher temperature allows the release of this disorder with further densification even if in both series the microstrain $\varepsilon$ was between $1 \times 10^{-5}$ and $4 \times 10^{-5}$, without a significant effect from the temperature. The average crystallite size increases by increasing the temperature for both series, as already observed.[30,40]

Some representative TEM micrographs with different magnifications of the YAGG:$Ce^{3+}$, $Cr^{3+}$, $Pr^{3+}$ samples prepared at $R$ = 0.25 and 1 after annealing in the range of 900−1400 °C are reported in Figure 5 and in Figure S1 with lower

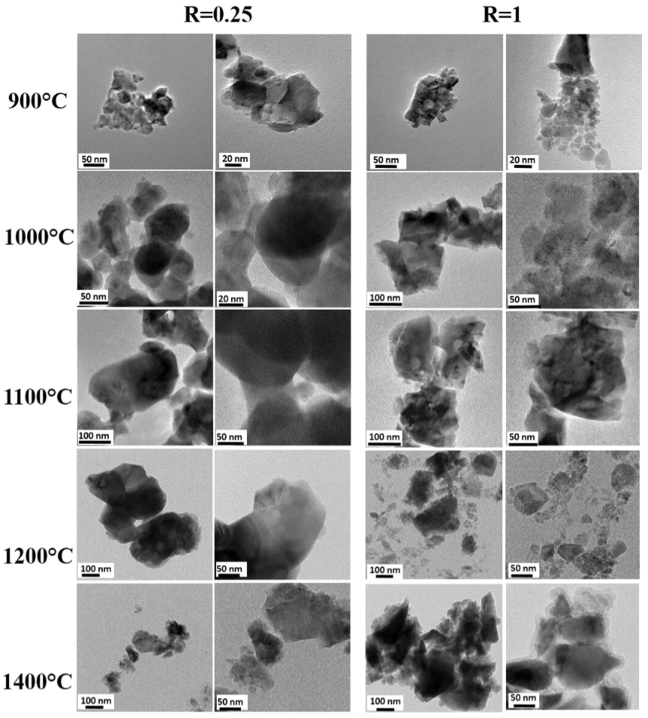


**Figure 5.** TEM micrographs at different magnifications of YAGG:$Ce^{3+}$,$Cr^{3+}$,$Pr^{3+}$ powders.

magnification. Two different enlargements have been chosen per sample to evidence primary nanoparticle distribution (low enlargements) and the details of each particle or aggregate (high enlargements).

TEM micrographs clearly show that the treatment at 900 °C causes the formation of agglomerates made of few YAGG particles not regular in shape. Particles of smaller size and more uniform in shape are formed starting from being gel-like at $R$ = 1. Similar results were obtained for Ce:YAG nanocrystals in a previous study of some of us, where $R$ = 1 was considered the best to obtain a more homogeneous material.[42] The annealing process at a higher temperature sharpens the nanoparticles' edges and evidences their irregular polyhedral shapes for all


https://doi.org/10.1021/acs.langmuir.2c00687
Langmuir 2022, 38, 11539−11549

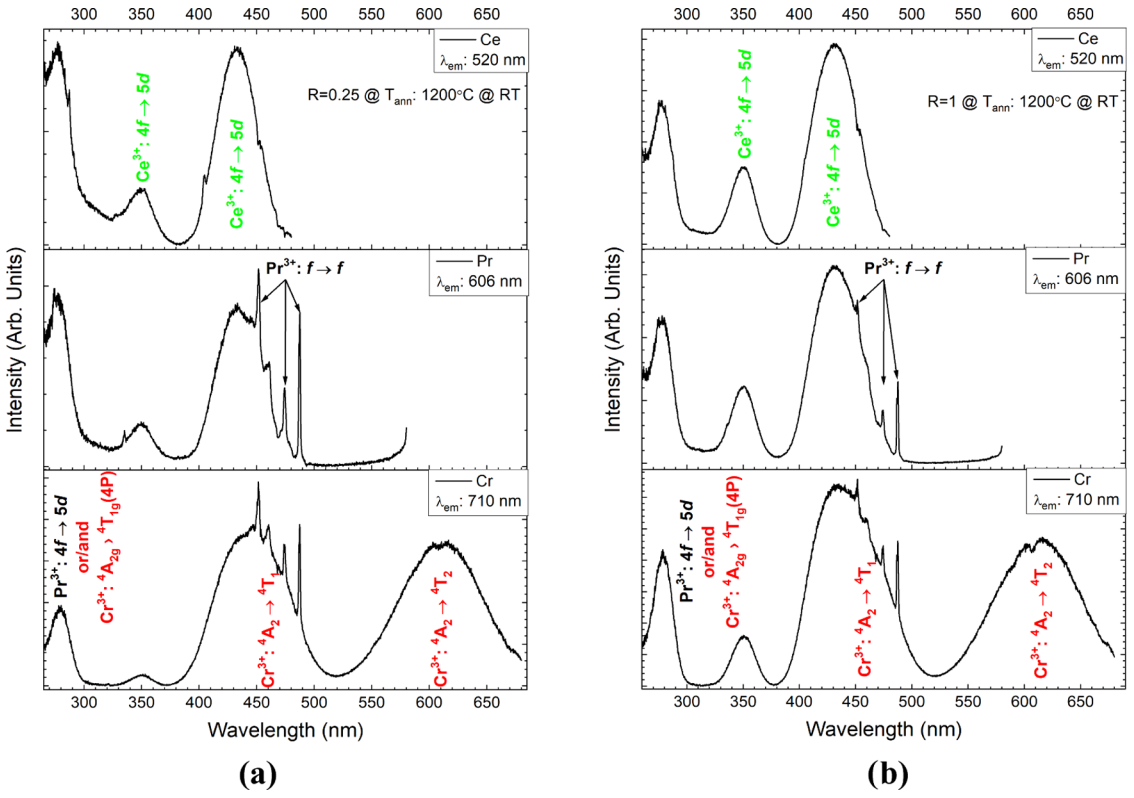


**Figure 6.** Photoluminescence excitation spectra of the YAGG:$Ce^{3+}$,$Cr^{3+}$,$Pr^{3+}$ powder synthesized at $R$ = 0.25 (a) and 1 (b) and calcined at 1200 °C.

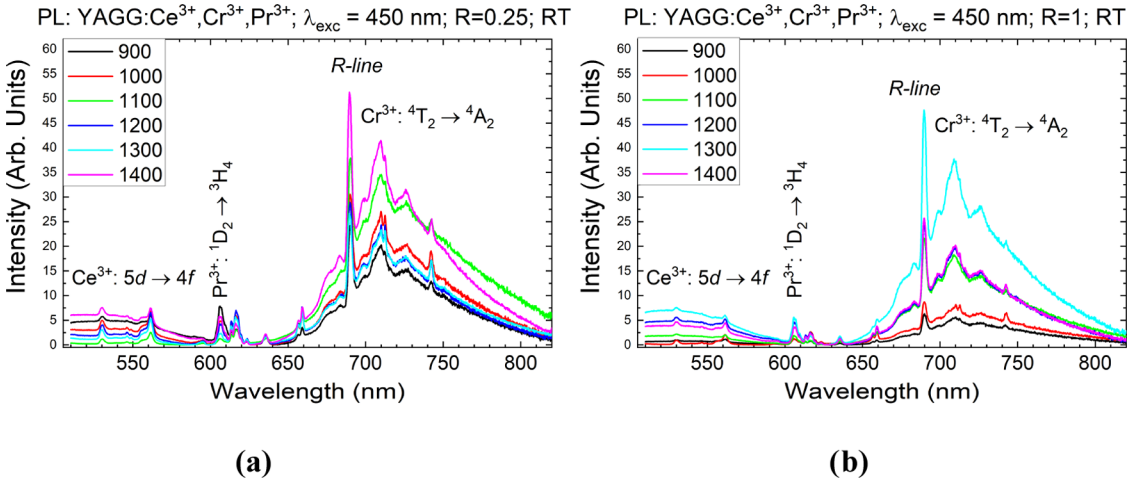


**Figure 7.** Photoluminescence spectra of the YAGG:$Ce^{3+}$,$Cr^{3+}$,$Pr^{3+}$ powder synthesized at $R$ = 0.25 (a) and 1 (b). $\lambda_{exc}$ = 450 nm at RT.

temperatures. The particle size increases with the temperature, as well as the crystalline size evaluated by XRPD data. However, the particle size is a little bit bigger than the crystalline size, and this can be explained considering that TEM permits to observe the details of the particles (with a polydispersion), while the XRPD technique evaluates the material in all volumes, giving an average of the crystalline size. The effect of $R$ is not so significant in the mean value of particle size. The crystalline nature of the particles has been evident in collecting the SAED patterns (reported in Figure S2a). All elements (Ga, Al, Y, Cr, Ce, Pr) are present in the EDS spectra (Figure S2b), and their ratio corresponds to the ones of the nominal composition.

**Photoluminescence.** To correlate the crystal structure parameters of the samples obtained at different synthesis conditions with the local structure of the dopant ions, which have a fundamental influence on their luminescence properties, selective studies by optical spectroscopy were carried out in the next step. In addition to the primary mechanism leading to PersL, which is the direct relaxation of the trapped energy due to irradiation into the luminescent ion, it is also possible to observe PersL resulting by exploiting in some cases the more likely energy transfer to the same ion through other dopants present in the material. Such an extended process to obtain a PersL signal can be studied in detail by analyzing the energy transfers, leading to normal photoluminescence occurring along, exactly, the same pathway. It is, therefore, crucial to


https://doi.org/10.1021/acs.langmuir.2c00687
Langmuir 2022, 38, 11539−11549

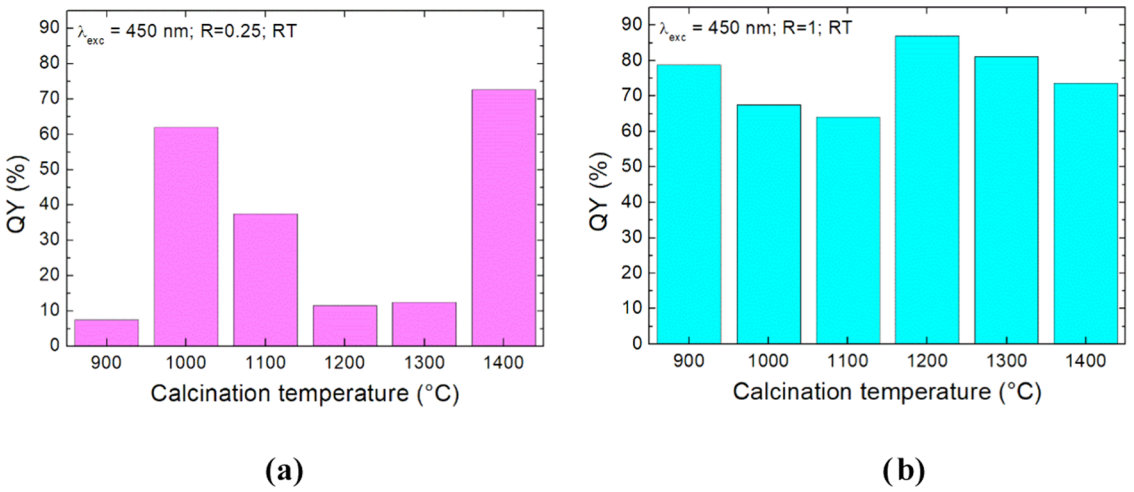


**Figure 8.** Quantum yields of the YAGG:$Ce^{3+}$,$Cr^{3+}$,$Pr^{3+}$ powder synthesized at $R$ = 0.25 (a) and 1 (b).

gather basic information about possible energy transfers with the help of the analysis of emission, excitation, and lifetime spectra of subsequent excited levels involved in these transfers.

The PLE spectra of the samples for $R$ = 0.25 and 1 are presented in Figures 6 and S3. The PLE spectra were acquired at $\lambda_{em}$ = 520, 606, and 710 nm (respectively for well-known $Ce^{3+}$, $Pr^{3+}$, and $Cr^{3+}$ emission peaks). All collected spectra show broad bands centered at 280, 350, and 435 nm, and a series of sharp lines at ∼450 nm additionally appeared in the PLE spectra of $Pr^{3+}$ and $Cr^{3+}$. A detailed analysis of energy transfer based on PLE spectra for this dopant system was carried out in our previous work.[40] Briefly, the band centered at 280 nm is assigned to $Pr^{3+}$:4f → 5d transition[50] and most likely the overlapping $Cr^{3+}$:$^4A_{2g}$ → $^4T_{1g}$(4P) transition.[37] The presence of this band also in the PLE spectrum of $Ce^{3+}$ indicates a pronounced ET from the lowest-lying 4f5d state of $Pr^{3+}$ to the 5d state of $Ce^{3+}$.[51] In the excitation spectra of $Ce^{3+}$ emission (520 nm), the two bands centered at 350 and 435 nm are attributed to the well-known splitting of the 4f → 5d $Ce^{3+}$ state by the crystal field.[52] In the excitation spectra of both $Pr^{3+}$ ($^1D_2$ → $^3H_4$, $\lambda_{em}$ = 606 nm) and $Cr^{3+}$ ($^4T_2$ → $^4A_2$, $\lambda_{em}$ = 710 nm), characteristic bands in the blue light range associated with f−f transitions of $Pr^{3+}$ were recorded. Additionally, in the PLE spectrum of $Cr^{3+}$, a typical $^4A_2$ → $^4T_2$ transition in the red range with a maximum at 617 nm was found.

The PL spectra acquired upon 350 nm excitation and presented in Figure S4 show a characteristic broad band corresponding to the d−f transition of $Ce^{3+}$ with a maximum centered at 512 nm and a sharper band with a maximum at 712 nm ($Cr^{3+}$:$^4T_2$ → $^4A_2$ transition). In between, less intensive but evident narrow lines are also present due to indirectly induced f−f transitions of $Pr^{3+}$:$^1D_2$ → $^3H_4$ (606 nm) and $^3P_0$ → $^3H_6$ (634 nm) evident upon 450 nm excitation (Figure 7).

In terms of practical application, the observed spectral characteristics and the possibility of obtaining efficient emission from all ions upon 450 nm excitation (Figure 7), which can be generated using commonly available LEDs, are very advantageous.[53,54] In general, an increase in the intensity of all bands was noticed as the annealing temperature increased for both $R$ = 0.25 and 1 samples. This behavior is a consequence of the fact that the surface-to-volume ratio decreases together with the decrease of the probability of nonradiative recombination through the elimination of quenching defects.[55,56] To find out which of the UGR synthesis parameters yields better results, affecting the final properties of PersL, it was necessary to study these aspects in more detail by analyzing the luminescence kinetics.

The luminescence lifetime is a very important parameter for understanding the quenching mechanisms related to many aspects of nonradiative relaxation of excited states depending mainly, but not exclusively, on the distance between dopant ions (their concentration), the local crystal field of the luminescence center and its distortions, grain size, effective refractive index, and the presence of the OH group.[55−57] On the other hand, it provides with the combined analysis of the excitation spectra an understanding of the excitation pathways between dopant ions. In view of this, the lifetimes for emission at 520 nm ($Ce^{3+}$:5d → 4f transition), 606 nm ($Pr^{3+}$:$^1D_2$ → 3H4 transition), and 690 nm ($Cr^{3+}$:$^4T_2$ → $^4A_2$ transition) after excitation at 350 nm (specific for $Ce^{3+}$) and 450 nm for exciting all ions at the same time were detected (Figures S5 and S6, respectively). Then, an effective (average) lifetime was calculated (Figure S7). From the profile of the lifetime $Ce^{3+}$ emission, it can be seen that increasing annealing temperatures has a slight impact on decreasing lifetime, which is related to crystalline size and has no significant effect on the energy transfer to $Pr^{3+}$ and $Cr^{3+}$. The average lifetime for $Pr^{3+}$ coincides with the values previously obtained for the garnet matrix[58] and confirms the affiliation of this band to the $^1D_2$ → $^3H_4$ transition. At the same time, it is worth noting that the lifetime may depend on many factors, and as we can see at annealing temperatures from 900 to 1100 °C, the number of hydroxyl groups,[30] which are the quenching centers, decreases but at the same time the so-called effective refractive index, which affects the rate of radiation processes from lanthanide ions, increases. As a result, depending on the contribution of both factors, one can observe first an increase in the lifetime with quenching and then its decrease to values typical for reference single crystals. The effect of the effective refractive index, which can also be related to the degree of agglomeration (in the case of powders) as well as to porosity (of optical ceramics) on the rate of radiation processes in luminescent materials, is quite well described in previous papers.[55,57] What is relevant here is only the information that with the increasing agglomeration of powders (or removal of porosity from ceramics) there is a shortening of the measured lifetime, finally


https://doi.org/10.1021/acs.langmuir.2c00687
Langmuir 2022, 38, 11539−11549

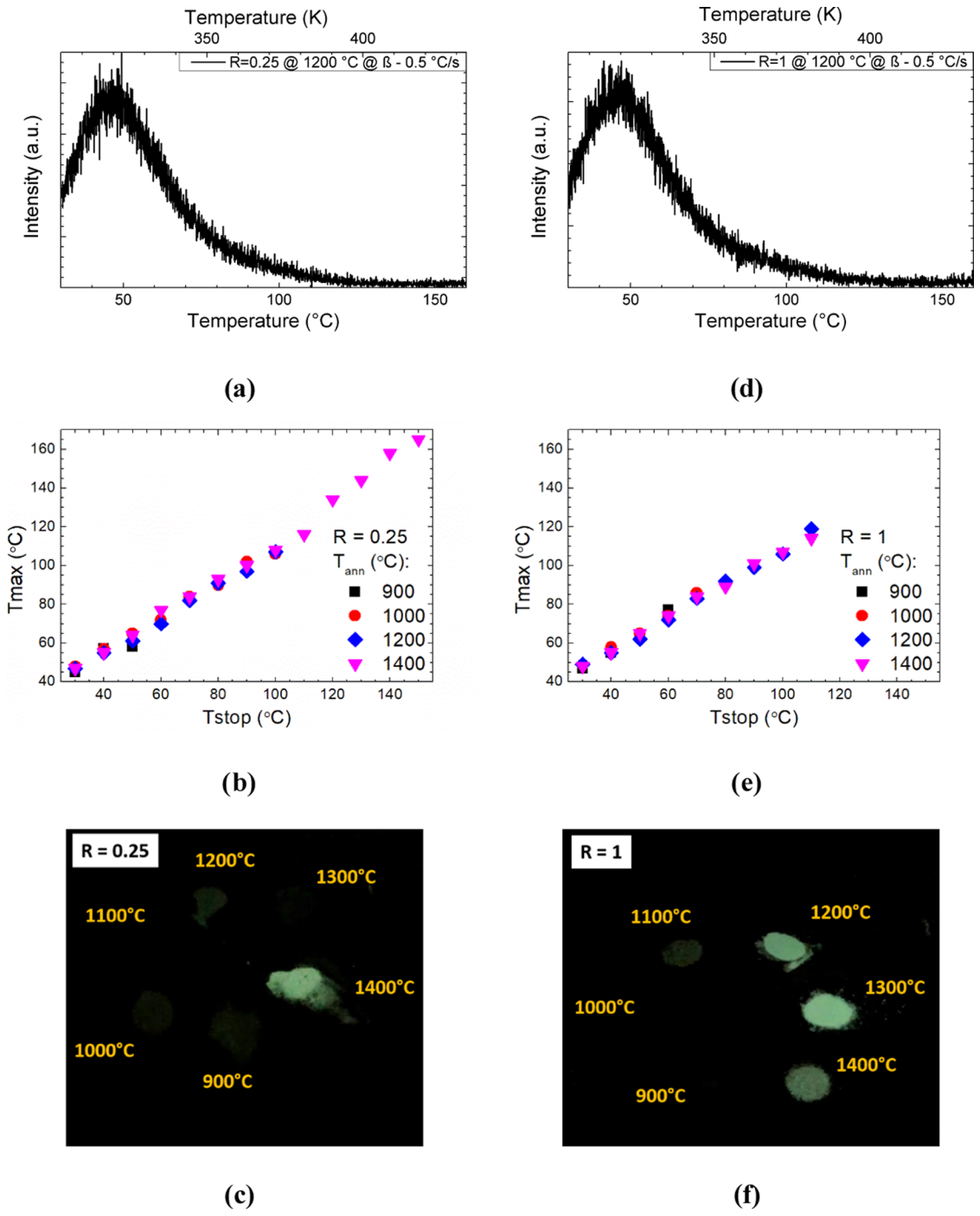


**Figure 9.** TL curve of the YAGG:$Ce^{3+}$,$Cr^{3+}$,$Pr^{3+}$ powder synthesized at $R$ = 0.25 (a) and 1 (d) and calcined at 1200 °C. Graphs of $T_{max}$ to $T_{stop}$ dependence (b, e), and the photograph of the obtained powder after UV irradiation (c, f).

to a value corresponding to the lifetime of the monocrystals of the compounds under consideration.

The QYs for all samples were detected after excitation at both 350 and 450 nm with an integrated sphere, and the obtained results are reported in Figures S8 and 8.

For both investigated series, quantum yields are very low for excitation at 350 nm (Figure S8). This may be because the total emission is only due to the transfer of energy from Ce to Pr and Cr. In the case of $\lambda_{exc}$ = 450 nm, the energies of all doped ions exited at the same time and QY are higher. In this case, for the $R$ = 0.25 series, no trend is observed with increasing calcination temperature. However, for the $R$ = 1 series for the same relation, more stable values of the quantum efficiency are observed with small deviations within the error limit. As we can see from Figure 8, the QY is maximal for an annealing temperature of 1200 °C.

**Thermoluminescence.** The TL curves have been acquired to obtain information about the traps in obtained nanophosphors and the effect of urea/metal molar ratios on the trap redistribution. The recorded TL curves (Figures 9 and S9) clearly show the main band with a maximum at ∼47 °C (∼320 K) and the additional band on the high-temperature side, which is not clearly pronounced against the background of the main band with a maximum of ∼87 °C (∼360 K). The general


https://doi.org/10.1021/acs.langmuir.2c00687
Langmuir 2022, 38, 11539−11549

shape of the TL curve is similar to that obtained previously for such structure syntheses with other methods.[30,40] For both urea/metal ratios ($R$), TL curves are quite symmetrical (except for the band on the high-temperature side), which indicates a homogeneous redistribution of traps with similar energy. Nevertheless, the contribution from the trap component with the TL maximum at around 47 °C is the most pronounced. However, these traps are not clearly separated, which may indicate the free transfer of electrons between them. For a more detailed analysis of the redistribution of traps and the nature of the additional band, a series of TL curves (Figure S10) was registered based on the method of precleaning traps, a so-called $T_{max}-T_{stop}$ method.[45]

Based on the obtained data, plots of $T_{max}$ versus $T_{stop}$ are drawn and presented in Figure 9b,e for $R$ = 0.25 and 1, respectively. The linear nature of the obtained curves with a line of a slope near 1.0 indicates that we have a series of first-order peaks. As the peaks overlap more, the interpretation tends toward the existence of a quasi-continuous distribution of peaks (and, therefore, of trapping centers).[59,60] As shown in the plots, the final release temperature for the sample synthesized at $R$ = 0.25 is 150 °C (for calcination temperature 1400 °C), while for $R$ = 1, it is 120 °C. As a result, long-term luminescence is registered only for nanoparticles with an annealing temperature of 1400 °C (Figures 9c and S11a). It should be noted that for samples synthesized at $R$ = 0.25, the slope was 0.65 ± 0.3 for nanoparticles annealed at 900 °C and approached 1 with increasing annealing temperature. It was 0.98 ± 0.03 for the sample annealed at 1400 °C. By comparing these data with the PersL of this series (Figures 9c and S11a), we can assume that there is a correlation between the glow and the degree of trap redistribution. In particular, we can expect that with a uniform quasi-continuous distribution of traps, the retrapping process is more uniform and thus contributes to long-term emission, while, for the series of single traps, the detrapping process will be uneven, and the recapture process will increase, resulting in increased losses and reduced afterglow time. In addition, the final release temperature for the sample synthesized at $R$ = 0.25 is 150 °C, while for $R$ = 1, it is 120 °C (in both cases when calcined at 1400 °C). This means that for $R$ = 0.25, there are traps with maxima at higher temperatures. At the same time, the samples synthesized at $R$ = 1 show a completely different trend of the slope in terms of trap redistribution based on $T_{max}-T_{stop}$ data analyses. The slope increases from 0.78 ± 0.1 to 0.98 ± 0.02 with increasing calcination temperature from 900 to 1200 °C and then begins to decrease to 0.85 ± 0.02 at 1400 °C, which in turn also correlates with the brightness of PersL (Figures 9f and S11b). Thus, the effect of $R$ on the resulting redistribution of traps is worth noting, namely, for $R$ = 1, it is possible to obtain nanophosphors with a smaller size of crystallites.

To analyze these traps, in addition to the $T_{max}-T_{stop}$ method, initial rise analyses[61] were used to determine the energies of each of the recorded curves. As a result, it was found that the activation energies for both series are the same and equal to around 0.75 ± 0.01 eV. Additionally, the analysis of the data using the initial rise method allowed the possibility for us to dedicate a series of traps with an energy of about 0.3 eV for a band from the high-temperature side for both samples. The existence of shallow traps can have an additional impact on the observed effects (PersL), and their nature may be directly related to structural changes, including surface defects.

The similarity of the activation energy for the samples from both series with different results with respect to the afterglow may indicate a nonlinear relationship between the depth of the trap and the efficiency of the glow, as previously reported.[40,62] By linking these results with the previous analysis of the structure and optical properties, it can be concluded with a high probability that despite traps with similar energy values, the intensity and duration of PersL may be influenced by other factors. In particular, morphology, phase change, redox reactions of the dopant ions, changes due to clustering of such dopants, and so on. However, this should be further established.

## CONCLUSIONS

The synthesis of YAGG:$Ce^{3+}$,$Cr^{3+}$,$Pr^{3+}$ crystallites with sizes starting from 45 nm by the urea glass route method (UGR) is successfully realized. UGR can be considered a more ecological, inexpensive, one-pot method with high yields, and therefore, it is suitable for large-scale production. The UGR method is relatively easy to carry out and gives results similar to other methods we have previously tested. The ratio of urea/metal salts, $R$, influences the formation of the gel-like, and for this study, we selected two systems at $R$ = 0.25 and 1. The gel-like prepared at $R$ = 0.5 was not selected because of a few differences in behavior observed between them. The two gel-like substances were then treated at 900, 1000, 1100, 1200, 1300, and 1400 °C for 1 h. From the structural and morphological point of view, there are no substantial differences in the cell parameters, crystallite size, and particle size with $R$. However, at the same $R$, the increase in size occurs with increasing temperature. At all temperatures, the composition of the powders respects the nominal ratio between atoms in the powders. Only some samples, treated at higher temperatures, showed efficient persistent luminescence. Regardless of synthesis parameters, we obtain nanopowders with long-term emission, which is associated with the presence of a series of first-order quasi-continuous distribution traps, which, in terms of applications, are important and contribute new knowledge. In potential biological applications and also in the field of luminescent labeling, not always duration and intensity are the most important criterion for their suitability. By changing the parameter $R$, it is possible to achieve a more uniform distribution of quasi-continuous traps, which in turn has a positive effect on obtaining PersL from phosphors in the nanoscale range. Additional maxima at the shoulder of high temperatures with an energy of around 0.3 eV are detected. This may be due to the presence of traps associated with structural imperfections in particular to the heterogeneous redistribution of dopant ions on the surface of the obtained nanophosphors.

## ASSOCIATED CONTENT

### Supporting Information

The Supporting Information is available free of charge at https://pubs.acs.org/doi/10.1021/acs.langmuir.2c00687.

TEM micrographs of YAGG:$Ce^{3+}$,$Cr^{3+}$,$Pr^{3+}$ powders calcinated at 1400 °C for 1 h (Figure S1); selected area electron diffraction (SAED) pattern and EDS analysis (Figure S2); photoluminescence excitation spectra as a function of calcination temperature for $R$ = 0.25 and 1 (Figure S3); photoluminescence spectra of YAGG:-$Ce^{3+}$,$Cr^{3+}$,$Pr^{3+}$ at $\lambda_{exc}$ = 350 nm (Figure S4); photo-



https://doi.org/10.1021/acs.langmuir.2c00687
Langmuir 2022, 38, 11539−11549

luminescence lifetimes of YAGG:$Ce^{3+}$,$Cr^{3+}$,$Pr^{3+}$ as a function of calcination temperature at $\lambda_{exc}$ = 350 (Figure S5); photoluminescence lifetimes of YAGG:-$Ce^{3+}$,$Cr^{3+}$,$Pr^{3+}$ as a function of calcination temperature at $\lambda_{exc}$ = 450 nm (Figure S6); average lifetime as a function of the calcination temperature and excitation and detection wavelengths (Figure S7); quantum yields of YAGG:$Ce^{3+}$,$Cr^{3+}$,$Pr^{3+}$ at $\lambda_{exc}$ = 350 nm (Figure S8); thermoluminescence curves of YAGG:$Ce^{3+}$,$Cr^{3+}$,$Pr^{3+}$ (Figure S9); thermoluminescence glow curves registered during $T_{max}$−$T_{stop}$ experiments (Figure S10); and persistent luminescence decay curve after irradiation by a blue laser diode $\lambda_{irr}$ − 450 nm (Figure S11)(PDF)

## AUTHOR INFORMATION


### Corresponding Authors

**Vitalii Boiko** − *Institute of Low Temperature and Structure Research, Polish Academy of Sciences, PL-50-422 Wrocław, Poland;* orcid.org/0000-0001-6652-7890; Email: v.boiko@intibs.pl

**Maria Luisa Saladino** − *Department of Biological, Chemical and Pharmaceutical Sciences and Technologies (STEBICEF) and INSTM UdR − Palermo, University of Palermo, IT-90128 Palermo, Italy;* orcid.org/0000-0002-7481-8556; Email: marialuisa.saladino@unipa.it

### Authors

**Francesco Armetta** − *Department of Biological, Chemical and Pharmaceutical Sciences and Technologies (STEBICEF) and INSTM UdR − Palermo, University of Palermo, IT-90128 Palermo, Italy;* orcid.org/0000-0002-7677-602X

**Federica Ursi** − *Department of Biological, Chemical and Pharmaceutical Sciences and Technologies (STEBICEF) and INSTM UdR − Palermo, University of Palermo, IT-90128 Palermo, Italy*

**Marta Markowska** − *Institute of Low Temperature and Structure Research, Polish Academy of Sciences, PL-50-422 Wrocław, Poland*

**Karina Grzeszkiewicz** − *Institute of Low Temperature and Structure Research, Polish Academy of Sciences, PL-50-422 Wrocław, Poland;* orcid.org/0000-0002-2007-8329

**Cecilia Mortalò** − *Institute of Condensed Matter Chemistry and Energy Technologies (ICMATE), National Research Council of Italy, IT-35127 Padova, Italy*

**Cristina Leonelli** − *Department of Engineering "Enzo Ferrari", University of Modena and Reggio Emilia, IT-41125 Modena, Italy*

**Dariusz Hreniak** − *Institute of Low Temperature and Structure Research, Polish Academy of Sciences, PL-50-422 Wrocław, Poland;* orcid.org/0000-0003-1384-2314

Complete contact information is available at: https://pubs.acs.org/10.1021/acs.langmuir.2c00687


### Notes

The authors declare no competing financial interest.

## ACKNOWLEDGMENTS

This work was supported by the Polish National Science Centre, Grant: OPUS 11 2016/21/B/ST5/02385 (to V.B., M.M., K.G., and D.H.) and the Central European Initiative (CEI) within the Know-how Exchange Programme (KEP), Grant Agreement No. 1206.007-18-CPMSC (to V.B., M.M., M.L.S., and D.H.). M.L.S. and D.H. thank the University of Palermo for the CORI2017 − Action D1 Project to have the possibility of visits between the two Institutions. F.U. thanks the University of Palermo for supporting his research work through the Erasmus+Student Mobility for Traineeships A.A. 2018−2019. K.G. thanks for financial support by the National Science Centre, Grant: ETIUDA doctoral scholarship no 2019/32/T/ST5/00484. The authors would like to thank Prof. Eugeniusz Zych for the fruitful discussion of the thermoluminescence results and Robert M. Kowalski for the technical assistance in decay time measurement in the nanosecond range.

## REFERENCES


(1) Kumar, P.; Singh, S.; Gupta, B. K. Future Prospects of Luminescent Nanomaterial Based Security Inks: From Synthesis to Anti-Counterfeiting Applications. *Nanoscale* **2016**, *8*, 14297−14340.

(2) Armetta, F.; Sibeko, M. A.; Luyt, A. S.; Martino, D. F. C.; Spinella, A.; Saladino, M. L. Influence of the Ce: YAG Amount on Structure and Optical Properties of Ce:YAG-PMMA Composites for White LED. *Z. Phys. Chem.* **2016**, *230*, 1219−1231.

(3) Sarkar, D.; Ganguli, S.; Samanta, T.; Mahalingam, V. Design of Lanthanide-Doped Colloidal Nanocrystals: Applications as Phosphors, Sensors, and Photocatalysts. *Langmuir* **2019**, *35*, 6211−6230.

(4) Wang, F.; Banerjee, D.; Liu, Y.; Chen, X.; Liu, X. Upconversion Nanoparticles in Biological Labeling, Imaging, and Therapy. *Analyst* **2010**, *135*, 1839.

(5) Yang, D.; Ma, P.; Hou, Z.; Cheng, Z.; Li, C.; Lin, J. Current Advances in Lanthanide Ion (Ln3+)-Based Upconversion Nanomaterials for Drug Delivery. *Chem. Soc. Rev.* **2015**, *44*, 1416−1448.

(6) Lu, Q.; Dong, H.; Hu, J.; Huang, L.; Zhang, Y.; Li, M.; Liu, M.; Li, Y.; Wu, C.; Li, H. Insight into the Effect of Ligands on the Optical Properties of Germanium Quantum Dots and Their Applications in Persistent Cell Imaging. *Langmuir* **2020**, *36*, 12375−12382.

(7) Gai, S.; Li, C.; Yang, P.; Lin, J. Recent Progress in Rare Earth Micro/Nanocrystals: Soft Chemical Synthesis, Luminescent Properties, and Biomedical Applications. *Chem. Rev.* **2014**, *114*, 2343−2389.

(8) Prodi, L.; Rampazzo, E.; Rastrelli, F.; Speghini, A.; Zaccheroni, N. Imaging Agents Based on Lanthanide Doped Nanoparticles. *Chem. Soc. Rev.* **2015**, *44*, 4922−4952.

(9) Singh, S. K. Red and near Infrared Persistent Luminescence Nano-Probes for Bioimaging and Targeting Applications. *RSC Adv.* **2014**, *4*, 58674−58698.

(10) Głuchowski, P.; Rajfur, K. Impact of the Synthesis Method on the Conventional and Persistent Luminescence in Gd3−XCexGa3Al2O12. *Inorg. Chem.* **2021**, *60*, 18777−18788.

(11) Armetta, F.; Saladino, M. L.; Martino, D. F. C.; Livreri, P.; Berrettoni, M.; Caponetti, E. Synthesis of Yttrium Aluminum Garnet Nanoparticles in Confined Environment II: Role of the Thermal Treatment on the Composition and Microstructural Evolution. *J. Alloys Compd.* **2017**, *719*, 264−270.

(12) Poelman, D.; Van der Heggen, D.; Du, J.; Cosaert, E.; Smet, P. F. Persistent Phosphors for the Future: Fit for the Right Application. *J. Appl. Phys.* **2020**, *128*, No. 240903.

(13) Castaing, V.; Arroyo, E.; Becerro, A. I.; Ocaña, M.; Lozano, G.; Míguez, H. Persistent Luminescent Nanoparticles: Challenges and Opportunities for a Shimmering Future. *J. Appl. Phys.* **2021**, *130*, No. 080902.

(14) Shirahata, N.; Hirakawa, D.; Masuda, Y.; Sakka, Y. Size-Dependent Color Tuning of Efficiently Luminescent Germanium Nanoparticles. *Langmuir* **2013**, *29*, 7401−7410.

(15) Mori, M.; Xu, J.; Okada, G.; Yanagida, T.; Ueda, J.; Tanabe, S. Scintillation and Optical Properties of Ce-Doped YAGG Transparent Ceramics. *J. Rare Earths* **2016**, *34*, 763−768.

(16) Fu, S.; Tan, J.; Bai, X.; Yang, S.; You, L.; Du, Z. Effect of Al/Ga Substitution on the Structural and Luminescence Properties of Y3(Al1-XGax)5O12: $Ce^{3+}$ Phosphors. *Opt. Mater.* **2018**, *75*, 619−625.

(17) Gilleo, M. A.; Geller, S. Substitution for Iron in Ferrimagnetic Yttrium-Iron Garnet. *J. Appl. Phys.* **1958**, *29*, 380−381.
(18) Nakatsuka, A.; Yoshiasa, A.; Yamanaka, T. Cation Distribution and Crystal Chemistry of Y3Al5-XGaxO12 ($0 \leq x \leq 5$) Garnet Solid Solutions. *Acta Crystallogr., Sect. B* **1999**, *55*, 266−272.
(19) Xu, J.; Tanabe, S. Persistent Luminescence Instead of Phosphorescence: History, Mechanism, and Perspective. *J. Lumin.* **2019**, *205*, 581−620.
(20) Boiko, V.; Zeler, J.; Markowska, M.; Dai, Z.; Gerus, A.; Bolek, P.; Zych, E.; Hreniak, D. Persistent Luminescence from Y3Al2Ga3O12 Doped with Ce3+ and Cr3+ after X-Ray and Blue Light Irradiation. *J. Rare Earths* **2019**, *37*, 1200−1205.
(21) Xu, J.; Ueda, J.; Kuroishi, K.; Tanabe, S. Fabrication of Ce3+−Cr3+ Co-Doped Yttrium Aluminium Gallium Garnet Transparent Ceramic Phosphors with Super Long Persistent Luminescence. *Scr. Mater.* **2015**, *102*, 47−50.
(22) Kim, J.; Lee, C. K.; Kim, Y. J. Low Temperature Synthesis of Lu3Al5-XGaxO12:Ce3+,Cr3+ Powders Using a Sol-Gel Combustion Process and Its Persistent Luminescence Properties. *Opt. Mater.* **2020**, *104*, No. 109944.
(23) Xu, J.; Tanabe, S.; Sontakke, A. D.; Ueda, J. Near-Infrared Multi-Wavelengths Long Persistent Luminescence of Nd3+ Ion through Persistent Energy Transfer in Ce3+,Cr3+ Co-Doped Y3Al2Ga3O12 for the First and Second Bio-Imaging Windows. *Appl. Phys. Lett.* **2015**, *107*, No. 081903.
(24) Dai, Z.; Boiko, V.; Markowska, M.; Gerus, A.; Grzeszkiewicz, K.; Hölsä, J.; Saladino, M. L.; Hreniak, D. Optical Studies of Y3(Al,Ga)5O12:Ce3+,Cr3+,Nd3+ Nano-Phosphors Obtained by the Pechini Method. *J. Rare Earths* **2019**, *37*, 1132−1136.
(25) Xu, J.; Murata, D.; Ueda, J.; Viana, B.; Tanabe, S. Toward Rechargeable Persistent Luminescence for the First and Third Biological Windows via Persistent Energy Transfer and Electron Trap Redistribution. *Inorg. Chem.* **2018**, *57*, 5194−5203.
(26) Maldiney, T.; Lecointre, A.; Viana, B.; Bessière, A.; Bessodes, M.; Gourier, D.; Richard, C.; Scherman, D. Controlling Electron Trap Depth to Enhance Optical Properties of Persistent Luminescence Nanoparticles for in Vivo Imaging. *J. Am. Chem. Soc.* **2011**, *133*, 11810−11815.
(27) Sharma, S. K.; Gourier, D.; Viana, B.; Maldiney, T.; Teston, E.; Scherman, D.; Richard, C. Persistent Luminescence in Nano-phosphors for Long Term in-Vivo Bio-Imaging. *SPIE Proc.* **2015**, *9337*, No. 93370I.
(28) Ueda, J.; Kuroishi, K.; Tanabe, S. Bright Persistent Ceramic Phosphors of Ce3+ - Cr3+ - Codoped Garnet Able to Store by Blue Light. *Appl. Phys. Lett.* **2014**, *104*, No. 101904.
(29) Dai, Z.; Boiko, V.; Grzeszkiewicz, K.; Saladino, M. L.; Li, J.; Hreniak, D. Effect of Annealing Treatment on the Persistent Luminescence of Y3Al2Ga3O12:Ce3+,Cr3+,Pr3+ Ceramics. *Opt. Mater.* **2020**, *105*, No. 109888.
(30) Dai, Z.; Boiko, V.; Grzeszkiewicz, K.; Markowska, M.; Ursi, F.; Hölsä, J.; Saladino, M. L.; Hreniak, D. Effect of Annealing Temperature on Persistent Luminescence of Y3Al2Ga3O12:Cr3+ Co-Doped with Ce3+ and Pr3+. *Opt. Mater.* **2020**, No. 110522.
(31) Wu, L.; Hu, J.; Zou, Q.; Lin, Y.; Huang, D.; Chen, D.; Lu, H.; Zhu, H. Synthesis and Optical Properties of a Y3(Al/Ga)-5O12:Ce3+,Cr3+,Nd3+persistent Luminescence Nanophosphor: A Promising near-Infrared-II Nanoprobe for Biological Applications. *Nanoscale* **2020**, *12*, 14180−14187.
(32) Xu, J.; Murata, D.; Ueda, J.; Tanabe, S. Near-Infrared Long Persistent Luminescence of Er3+ in Garnet for the Third Bio-Imaging Window. *J. Mater. Chem. C* **2016**, *4*, 11096−11103.
(33) Xu, J.; Ueda, J.; Tanabe, S. Novel Persistent Phosphors of Lanthanide−Chromium Co-Doped Yttrium Aluminum Gallium Garnet: Design Concept with Vacuum Referred Binding Energy Diagram. *J. Mater. Chem. C* **2016**, *4*, 4380−4386.
(34) Wang, B.; Lin, H.; Yu, Y.; Chen, D.; Zhang, R.; Xu, J.; Wang, Y. Ce3+/Pr3+: YAGG: A Long Persistent Phosphor Activated by Blue-Light. *J. Am. Ceram. Soc.* **2014**, *97*, 2539−2545.
(35) Feng, S.; Qin, H.; Wu, G.; Jiang, H.; Zhao, J.; Liu, Y.; Luo, Z.; Qiao, J.; Jiang, J. Spectrum Regulation of {YAG}:{Ce} Transparent Ceramics with {Pr}, {Cr} Doping for White Light Emitting Diodes Application. *J. Eur. Ceram. Soc.* **2017**, *37*, 3403−3409.
(36) Boiko, V.; Markowska, M.; Consentino, L.; Saladino, M. L.; Hreniak, D. Effect of Ce3+ Concentration on Persistent Luminescence of YAGG:Ce3+,Cr3+,Nd3+ Nanophosphors Obtained by the Co-Precipitation Method. *Opt. Mater.* **2020**, *107*, No. 109956.
(37) Ueda, J.; Dorenbos, P.; Bos, A. J. J.; Kuroishi, K.; Tanabe, S. Control of Electron Transfer between Ce3+ and Cr3+ in the Y3Al5−xGaxO12 Host via Conduction Band Engineering. *J. Mater. Chem. C* **2015**, *3*, 5642−5651.
(38) Chen, D.; Zhou, Y.; Xu, W.; Zhong, J.; Huang, P. Persistent and Photo-Stimulated Luminescence in Ce3+/Cr3+ Activated Y3Al2Ga3O12 Phosphors and Transparent Phosphor-in-Glass. *J. Mater. Chem. C* **2016**, *4*, 11457−11464.
(39) Ueda, J.; Katayama, M.; Asami, K.; Xu, J.; Inada, Y.; Tanabe, S. Evidence of Valence State Change of Ce3+ and Cr3+ during UV Charging Process in Y3Al2Ga3O12 Persistent Phosphors. *Opt. Mater. Express* **2017**, *7*, 2471.
(40) Boiko, V.; Dai, Z.; Markowska, M.; Leonelli, C.; Mortalò, C.; Armetta, F.; Ursi, F.; Nasillo, G.; Saladino, M. L.; Hreniak, D. Particle Size-Related Limitations of Persistent Phosphors Based on the Doped Y3Al2Ga3O12 System. *Sci. Rep.* **2021**, *11*, No. 141.
(41) Giordano, C.; Antonietti, M. Synthesis of Crystalline Metal Nitride and Metal Carbide Nanostructures by Sol−Gel Chemistry. *Nano Today* **2011**, *6*, 366−380.
(42) Armetta, F.; Saladino, M. L.; Giordano, C.; Defilippi, C.; Marciniak, Ł.; Hreniak, D.; Caponetti, E. Non-Conventional Ce:YAG Nanostructures via Urea Complexes. *Sci. Rep.* **2019**, *9*, No. 3368.
(43) Rietveld, H. M. *The Rietveld Method* Young, R. A., Ed.; Oxford University Press Inc.: Chester, 1995.
(44) Lutterotti, L.; Gialanella, S. X-Ray Diffraction Characterization of Heavily Deformed Metallic Specimens. *Acta Mater.* **1998**, *46*, 101−110.
(45) McKeever, S. W. S. *Thermoluminescence of Solids*, Cambridge University Press, 1985.
(46) Van den Eeckhout, K.; Bos, A. J. J.; Poelman, D.; Smet, P. F. Revealing Trap Depth Distributions in Persistent Phosphors. *Phys. Rev. B* **2013**, *87*, No. 045126.
(47) Jiang, L.; Zhang, X.; Zhu, S.; Tang, H.; Li, Q.; Zhang, W.; Mi, X.; Lu, L.; Liu, H.; Liu, X. Preparation and Luminescence Properties of Y3−yAl5−xGaxO12:Ce3+y Phosphors. *J. Mater. Sci.: Mater. Electron.* **2018**, *29*, 9045−9051.
(48) Liou, B.-T.; Yen, S.-H.; Kuo, Y.-K. Vegard's Law Deviation in Band Gaps and Bowing Parameters of the Wurtzite III-Nitride Ternary Alloys. *Proc. SPIE* **2005**, *5628*, 296.
(49) Chaika, M. A.; Tomala, R.; Strek, W.; Hreniak, D.; Dluzewski, P.; Morawiec, K.; Mateychenko, P. V.; Fedorov, A. G.; Doroshenko, A. G.; Parkhomenko, S. V.; Lesniewska-Matys, K.; Podniesinski, D.; Kozłowska, A.; Mancardi, G.; Vovk, O. M. Kinetics of Cr3+ to Cr4+ Ion Valence Transformations and Intra-Lattice Cation Exchange of Cr4+ in Cr,Ca:YAG Ceramics Used as Laser Gain and Passive Q-Switching Media. *J. Chem. Phys.* **2019**, *151*, No. 134708.
(50) Cavalli, E.; Esposito, L.; Bettinelli, M.; Speghini, A.; Ivanovskikh, K. V.; Hughes-Currie, R. B.; de Jong, M. YAG:Pr3+ Transparent Ceramics for Applications in Photonics: Synthesis and Characterization. *Mater. Res. Express* **2014**, *1*, 045903.
(51) Wang, L.; Zhang, X.; Hao, Z.; Luo, Y.; Zhang, J.; Wang, X. J. Interionic Energy Transfer in Y3Al5O12:Ce3+, Pr3+ Phosphor. *J. Appl. Phys.* **2010**, *108*, No. 093515.
(52) Yang, T.; Jiang, H.; Hai, O.; Dong, Y.; Liu, S.; Gao, S. Effect of Oxygen Vacancies on the Persistent Luminescence of Y3Al2Ga3O12:-Ce3+,Yb3+Phosphors. *Inorg. Chem.* **2021**, *60*, 17797−17809.
(53) Gao, Q.; Li, C.; Liu, Y.; Zhang, J.; Wang, X. J.; Liu, F. Manipulating Trap Filling of Persistent Phosphors upon Illumination by Using a Blue Light-Emitting Diode. *J. Mater. Chem. C* **2020**, *8*, 6988−6992.


https://doi.org/10.1021/acs.langmuir.2c00687
*Langmuir* 2022, 38, 11539−11549

(54) Lin, H.; Wang, B.; Huang, Q.; Huang, F.; Xu, J.; Chen, H.; Lin, Z.; Wang, J.; Hu, T.; Wang, Y. Lu2CaMg2(Si1−xGex)3O12:Ce3+ Solid-Solution Phosphors: Bandgap Engineering for Blue-Light Activated Afterglow Applicable to AC-LED. *J. Mater. Chem. C* **2016**, *4*, 10329−10338.
(55) Hreniak, D.; Stręk, W.; Głuchowski, P.; Bettinelli, M.; Speghini, A. The Influence of the Specific Surface of Grains on the Luminescence Properties of Nd3+-Doped Y3Al5O12 Nanopowders. *Appl. Phys. B* **2008**, *91*, 89−93.
(56) Hari Krishna, R.; Nagabhushana, B. M.; Nagabhushana, H.; Murthy, N. S.; Sharma, S. C.; Shivakumara, C.; Chakradhar, R. P. S. Effect of Calcination Temperature on Structural, Photoluminescence, and Thermoluminescence Properties of $Y_2O_3:Eu^{3+}$ Nanophosphor. *J. Phys. Chem. C* **2013**, *117*, 1915−1924.
(57) Głuchowski, P.; Małecka, M.; Stręk, W.; Ryba-Romanowski, W.; Solarz, P. Size Effect in Novel Red Efficient Garnet Nanophosphor. *J. Phys. Chem. C* **2017**, *121*, 25561−25567.
(58) Kowalski, R. M.; Komar, J.; Solarz, P. On the Combination of Praseodymium and Cerium, a New Concept of Improving Orange-Red Luminescence. *J. Alloys Compd.* **2020**, *848*, No. 156228.
(59) McKeever, S. W. S. On the Analysis of Complex Thermoluminescence. Glow-Curves: Resolution into Individual Peaks. *Phys. Status Solidi A* **1980**, *62*, 331−340.
(60) Sójka, M.; Zeler, J.; Zych, E. Effect of Ge:Si Ratio and Charging Energy on Carriers Trapping in Y2(Ge,Si)O5:Pr Powders Observed with Thermoluminescence Methods. *J. Alloys Compd.* **2021**, *858*, No. 157676.
(61) Bos, A. J. J. Theory of Thermoluminescence. *Radiat. Meas.* **2006**, *41*, S45−S56.
(62) Mashangva, M.; Singh, M. N.; Singh, T. B. Estimation of Optimal Trapping Parameters Relevant to Persistent Luminescence. *Indian J. Pure Appl. Phys.* **2011**, *49*, 583−589.




https://doi.org/10.1021/acs.langmuir.2c00687
*Langmuir* 2022, 38, 11539−11549